Winni Decking
DESY -MPY-
14/6/99

New Dog-bone Damping Ring Lattice

The following table summarizes the main requirements for the positron damping ring, both for the old TESLA parameters (according to the CDR) and for the new set of parameters.

	CDR	new set	determined by
hor. extracted emittance $\gamma\varepsilon_x$	12×10^{-6} m	8×10^{-6} m	luminosity
hor. equilibrium emittance $\gamma\varepsilon_x$	12×10^{-6} m	8×10^{-6} m	luminosity
ver. extracted emittance $\gamma\varepsilon_x$	0.2×10^{-6} m	0.02×10^{-6} m	luminosity
ver. equilibrium emittance $\gamma\varepsilon_x$	0.1×10^{-6} m	0.01×10^{-6} m	luminosity
equilibrium bunch length σ_z	< 0.01 m	< 0.01 m	bunch compressor
equilibrium momentum spread σ_p/P_0	≈ 0.1 %	≈ 0.1 %	bunch compressor
transverse acceptance $\gamma A_{x,y}$	> 0.05 m	> 0.05 m	$> 5 \times \gamma\varepsilon_{x,y;inj.}$
momentum acceptance A_p	> 0.5 %	> 0.5 %	
cycle time T_c	200×10^{-3} s	200×10^{-3} s	repetition rate
transverse damping time $\tau_{D;x,y}$	35×10^{-3} s	29×10^{-3} s	repetition rate, $\varepsilon_{inj.}$
bunch spacing $\Delta\tau_b$	50×10^{-9} s	20×10^{-9} s	kicker raise/fall time
number of bunches n_b	1130	2820	bunch train
number of particles per bunch N_e	3.6×10^{10}	2×10^{10}	luminosity

The main changes are the smaller vertical emittance and the shorter bunch spacing. The envisioned emittance coupling of $\approx$ 0.1% has been achieved already in synchrotron light sources.

One of the major problems we see is the incoherent tune shift due to space charge forces:

$$\Delta Q_{y;incoh} \approx -\frac{r_e N_e L_{ring}}{(2\pi)^{3/2}\sqrt{\varepsilon_x \varepsilon_y}\sigma_z \gamma^2} \tag{1}$$

with L_{ring} the ring length and $\varepsilon_{x,y}$ normalized emittances. $\Delta Q_{y;incoh}$ is ≈ 0.2 for the CDR parameter set and would get up to 0.43 for the new parameter set, assuming unchanged bunch length and energy. An obvious cure is to increase the damping ring energy. A new lattice has been designed which should be scalable to higher energies.

The redesign of the lattice is concentrated on the arcs. In the original proposed damping ring, the arcs contribute $\approx$ 20% of the total ring emittance. As most of the damping is provided by the wigglers, the emittance contribution of the arcs scales roughly like γ^6, approaching γ^3 as more and more damping occurs in the arcs.

The redesign of the arc lattice incorporates a change from the original FODO cells to so-called theoretical emittance (TME) cells. These cells have the basic property that the horizontal beta- and dispersion function have a minimum in the middle of the dipole. The minimum achievable emittance in a cell with given bending angle θ_{cell} is:

$$\epsilon_{x,min} = F(lattice, \nu_x)\frac{\gamma^2}{J_x}\theta_{cell}^3 \tag{2}$$

with $F(lattice, \nu_x)$ a function of the chosen lattice and phase advance per cell. A numerical calculation of the minimum emittance for different phase advances in the FODO and TME lattice is shown in figure 1.

The optimum horizontal phase advance for minimum emittance is usually not reached in real lattices. The strong focusing required leads to unacceptable dynamical behavior. A typical phase advance for a FODO cell is $\nu_{x;FODO} = 0.25$. The thus reached emittance is only 2 times larger than the smallest reachable one. For a TME lattice $\nu_{x;TME} = 0.4$ seems to be a reasonable compromise. The minimum emittance is missed by roughly a factor of four. For these phase advances, a TME cell gives a ≈ 6 times smaller emittance for the same bending angle per cell, or a $\approx 6^{\frac{1}{3}}$ larger bending angle leads to the same emittance.

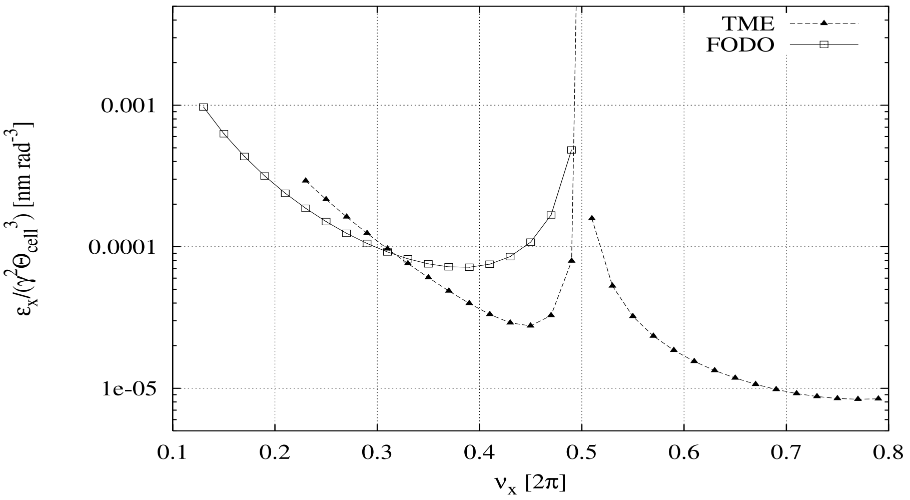

Figure 1: Comparison of minimum emittance, normalized to $\gamma^2\theta_{cell}^3$ for TME and FODO cell.

The simplest TME cell can be made from a horizontally defocusing combined function dipole flanked by two focusing quadrupoles. The advantages of this cell is a small number of elements per cell, small space requirements, and a change of the damping partition numbers in the 'right' direction. The disadvantages are no flexibility once the magnets are built and a poor separation of horizontal and vertical $\beta-$functions in view of the chromaticity correction. The advantage of shifting the damping partition numbers is negligible in the dog-bone damping ring, as most of the damping is provided by the wigglers. Because of these reasons we have chosen a separate function dipole flanked by quadrupole doublets. This gives flexibility in changing the phase advance if desired. The drift space between the two outer, focusing quadrupoles provides space for the focusing sextupole at highest horizontal dispersion and beta-function (see figure 2).

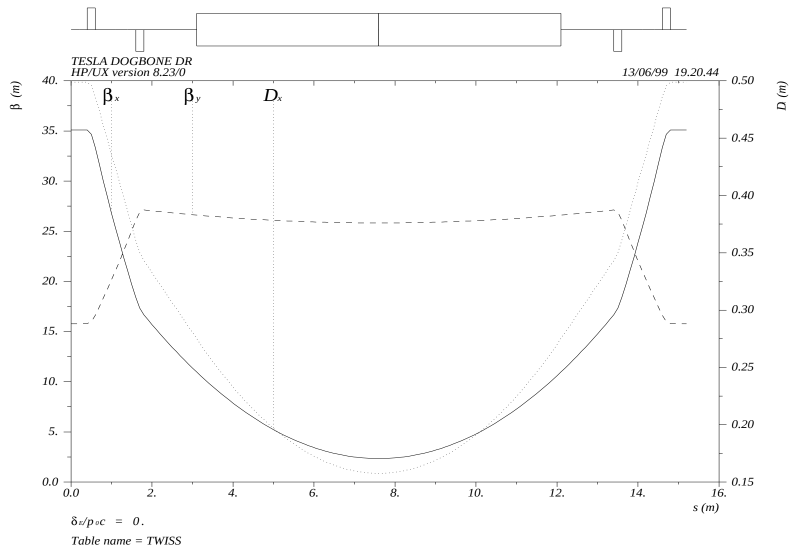

Figure 2: ARC bending magnet cell.

The remaining parameter is the length of the dipole magnet $L_{dip.}$. The optimum values for the minimum of the horizontal beta and dispersion function in the middle of the dipole

Table 1: Summary of the new damping ring parameters

energy	5.0 GeV
circumference	17 km
arc length	920 m
hor./ver. tunes Q_x, Q_y	71.85 , 38.71
hor./ver. chromaticities ξ_x, ξ_y	-120 , -62
hor. equilibrium emittance $\gamma\varepsilon_x$	9×10^{-6} m
transverse damping time $\tau_{D;x,y}$	28×10^{-3} s
transverse acceptance $\gamma A_{x,y}$	0.05 m
equilibrium bunch length σ_z	6 mm
equilibrium momentum spread σ_p/P_0	0.13 %
longitudinal damping time $\tau_{D;s}$	14×10^{-3} s
energy loss per turn U_0	20.3 MeV
rf-voltage U_{rf}	50 MV
momentum compaction α	0.12×10^{-3}
wiggler field $B_{wiggler}$	1.5 T
wiggler period length $\lambda_{wiggler}$	0.4 m
total wiggler length	288 m

of a TME cell scale with the dipole length:

$$\beta_{x,min} = \frac{1}{2\sqrt{15}} L_{dip.} \qquad\qquad \eta_{x,min} = \frac{\theta L_{dip.}}{24} \tag{3}$$

These values also scale roughly with the ratio of the reached emittance to the minimum possible emittance. We have chosen a rather long dipole magnet. This gives the disadvantage of increased arc- and thus tunnel-length. The benefits are larger optical functions, which lead to smaller sextupole strength and thus better dynamic properties of the lattice. Another parameter which can be controlled through the cell length is the momentum compaction factor α. The bunch length should be small (< 1 cm), but not to small, as this influences single bunch instabilities as well as the incoherent space charge tune shift. The momentum compaction factor is:

$$\alpha = \frac{1}{L_{ring}} \int\limits_{dipoles} \frac{\eta}{\rho} ds \approx \frac{4\pi}{L_{ring}} \theta_{dip.} L_{dip.} G(lattice, \nu_x) \tag{4}$$

for the dog-bone damping ring with two 2π arcs. G is another function depending on the chosen lattice type.

We have designed a TME cell with a bending angle of $\theta_{cell} = 12$ deg, which compares with the bending angle of $\theta_{cell} = 7.5$ deg for the FODO cell used in the original damping ring lattice. The dipole length has been set to 9 m to reach a comparable momentum compaction. The phase advance has been chosen to $\nu_x = 0.4$, $\nu_y = 0.1$. The resulting ring shows a two times larger dynamic aperture. Thus a change towards a TME lattice is even without an increase in energy desirable.

To avoid problems with the space charge tune shift the number of TME cells has been doubled (bending angle halved) without changing the dipole length. This allows an energy increase of a factor of $1.4 - 2$. As more damping is provided in the arcs, the wiggler length can also be reduced. The resulting parameters of the new ring are summarized in table 1. The incoherent tune shift is reduced to 0.24.

Figure 2 shows the arc cell with a 6 deg bending magnet. The sextupoles are placed at the end/beginning of the cell and close to the defocusing quadrupole.

The transformation between the positive and negative bending area is done via a zero dispersion FODO lattice. The length is adjusted to provide ≈ 0.5 m space between the two beam lines in the linac tunnel. The dispersion compression consists out of one half dipole.

The same compressor is used for the matching in the wiggler cell. Figure 3 displays the section between the positive and negative bending area together with the dispersion compressor.

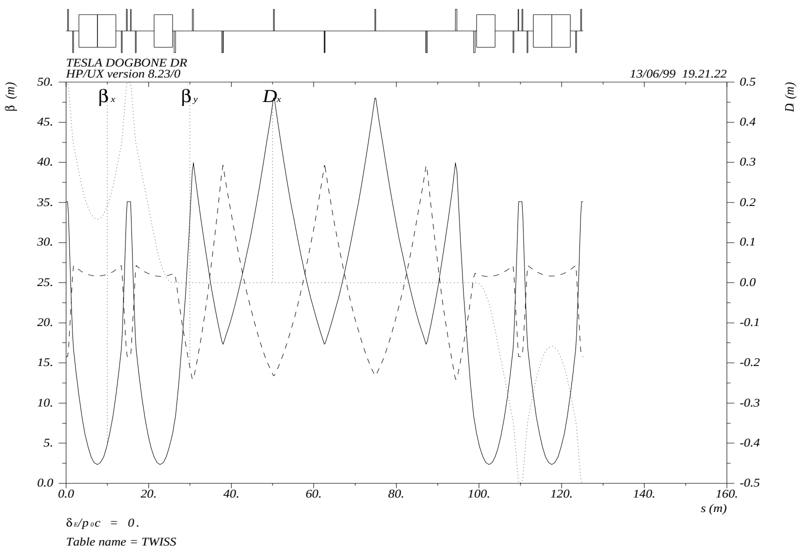

Figure 3: Transformation between positive and negative bending cell.

The basic wiggler cell is unchanged compared to the CDR. It consists out of 10 m long FODO cells with a phase advance of $\nu_x = 0.166$, $\nu_y = 0.125$. The wiggler strength has been kept at 1.5 T in order to keep the wiggler short. Figure 4 shows a wiggler cell, while figure 5 shows the match between the wiggler section and the arc section.

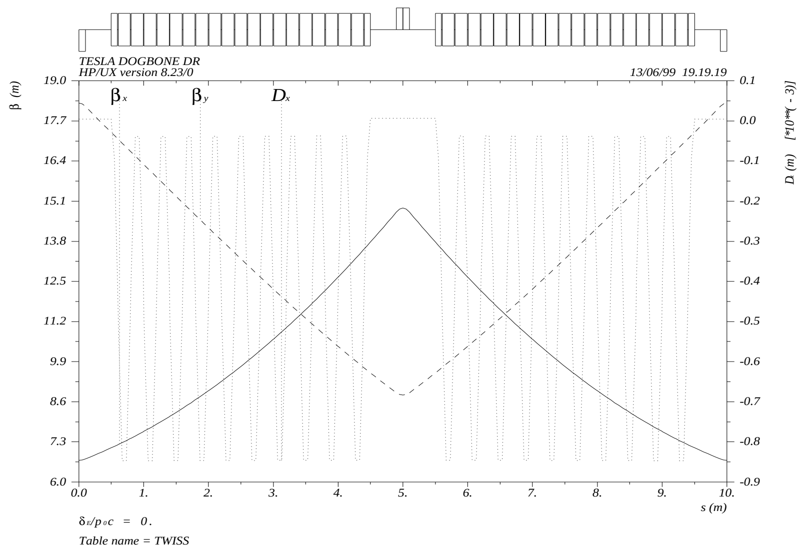

Figure 4: Wiggler cell.

The long straight section cells consist of long FODO cells. Their length has been adjusted to provide a 17 km long ring. The phase advance has been set to $\nu_{x,y} = 0.125$, which yields a maximum beta-function of ≈ 200 m. Together with the smaller injected emittance due to the energy increase this still provides enough physical aperture. Figure 6 shows a straight section cell and the matching into the wiggler section.

A MAD deck of the complete ring can be found at
http://www.desy.de/˜wdecking/dog/DOG2.1.

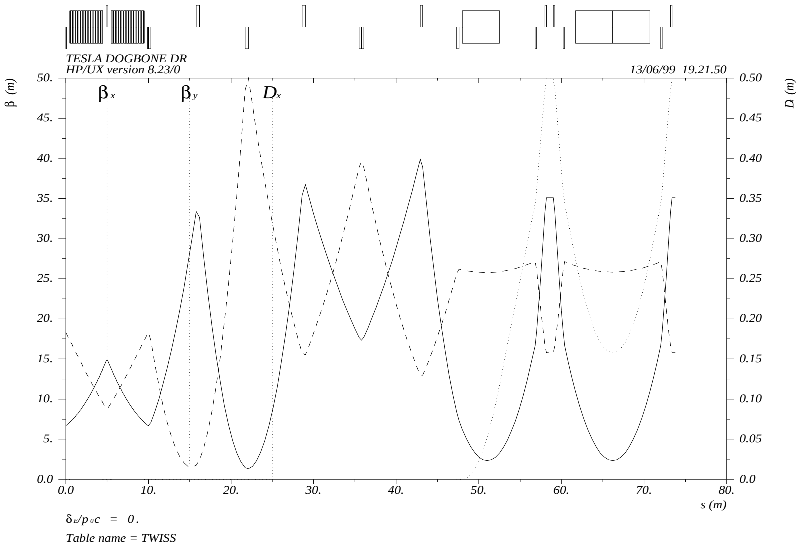

Figure 5: Matching between wiggler cell and arc.

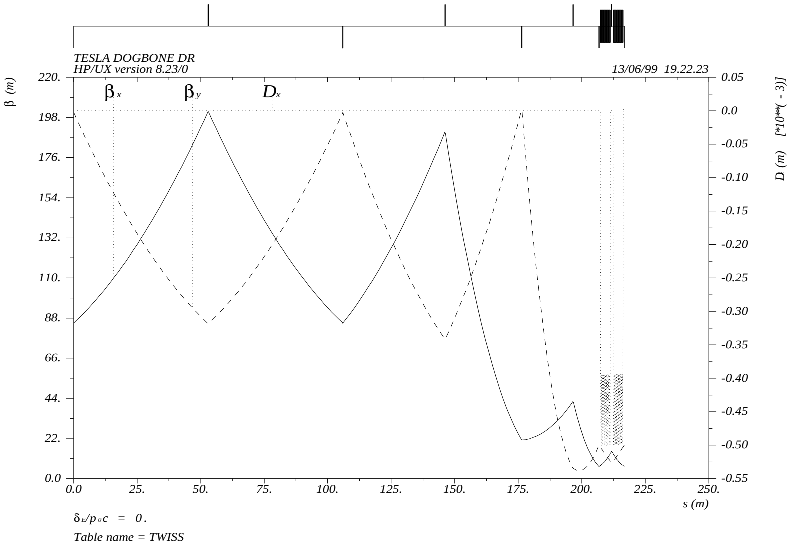

Figure 6: Matching between straight section and wiggler cell.